van der Waals vibrational dependence in the vibrational predissociation dynamics of OH–Ar

Mary T. Berry, Mitchell R. Brustein, and Marsha I. Lester

Citation: J. Chem. Phys. **92**, 6469 (1990); doi: 10.1063/1.458327
View online: http://dx.doi.org/10.1063/1.458327
View Table of Contents: http://jcp.aip.org/resource/1/JCPSA6/v92/i11
Published by the AIP Publishing LLC.

van der Waals vibrational dependence in the vibrational predissociation dynamics of OH–Ar

Mary T. Berry, Mitchell R. Brustein, and Marsha I. Lester[a)]
Department of Chemistry, The University of Pennsylvania, Philadelphia, Pennsylvania 19104-6323

(Received 13 December 1989; accepted 19 February 1990)

The OH–Ar vibrational predissociation lifetimes and OH product rotational state distributions are shown to change with van der Waals (vdW) state selection within the manifold of OH–Ar vibrational states correlating with OH $A\,^2\Sigma^+$ ($v' = 1$) + Ar($^1S_0$). Excitations to pure vdW stretching levels result in similar product state distributions, but predissociation lifetimes that vary from 30 ± 8 ps at $v'_{vdW} = 0$ to greater than 150 ps at $v'_{vdW} = 6$. Excitations to assigned vdW bend-stretch combination bands result in product state distributions which differ from those observed after excitation of the pure vdW stretch and those differences are attributed to the form of the bending wave function. Rotational constants and band positions for OH–Ar features in the OH $A\,^2\Sigma^+$–$X\,^2\Pi_{3/2}$ 0–0, 1–0, 1–1, 2–1, 1–2, and 2–2 regions are also presented. The spectroscopic analysis reveals details about the radial portion of the intermolecular potential between Ar ($^1S_0$) and hydroxyl radicals in the ground $X\,^2\Pi_{3/2}$ and excited $A\,^2\Sigma^+$ states. Vibrational excitation of the OH moiety induces measurable perturbations in the interaction potentials along the OH–Ar vdW stretching coordinate for both electronic states. These changes are reflected in the vibrational predissociation rates.

INTRODUCTION

A wealth of information on the attractive and repulsive forces between atoms and molecules has been derived from scattering experiments and spectroscopic studies of weakly bound van der Waals (vdW) complexes. Most experiments have been conducted on closed-shell molecular species and, until recently, little was known about the interaction potentials in open shell systems.[1–9] Scattering experiments have probed the interatomic potentials between open shell atoms, such as F and O,[6–8] with rare gas partners. The interaction between the hydroxyl radical and an argon atom provides a model case for examining the intermolecular potential in an open-shell system[9] since the OH–Ar complex is both experimentally observable and theoretically tractable. The determination of the interaction potentials between the hydroxyl radical and various collision partners is also of practical importance because of the key role of hydroxyl radicals in combustion and atmospheric chemistry.

OH in association with Ar has been studied under a wide range of experimental conditions: supersonic free jets,[10–15] gas bulbs,[16,17] and rare gas matrices.[18] Goodman and Brus[18] first identified a low-frequency vibrational mode upon electronic excitation of hydroxyl radicals imbedded in an argon matrix. Anharmonic vibrational progressions, consisting of five or six members, were observed in the region about the OH $A\,^2\Sigma^+$–$X\,^2\Pi_{3/2}$ 0–0, 1–0, and 2–0 transitions using laser-induced fluorescence. The vibrational motion was attributed to a stretch which involves OH $A\,^2\Sigma^+$ interacting strongly with a single Ar nearest neighbor. A vibrational analysis showed that OH was much more deeply bound to Ar when in the excited $A\,^2\Sigma^+$ state and that the OH–Ar bond length was substantially reduced ($\Delta r_e = 1.15$ Å) in the excited state.

Collisional studies at thermal energies ($\approx 200\ cm^{-1}$) of hydroxyl radicals in the $A\,^2\Sigma^+$ state with Ar and a variety of other partners have shown that attractive, long-range forces dominate the relaxation dynamics.[16] Vibrational energy transfer cross sections were found to be on the order of gas kinetic values and decreased sharply with increasing rotational level. The high efficiency of the inelastic energy transfer processes has been attributed to the formation of a transitory "collision complex" in the entrance channel of the potential energy surface, while the rotational level dependence indicated an anisotropy in the attractive forces.[19]

The intermolecular potential between OH and Ar in the gas phase can be examined in more detail by aggregating the collision partners in a vdW complex. In this laboratory, laser-induced fluorescence[10,11] and infrared overtone spectroscopy[13] of the OH–Ar complex have been used to examine the attractive well regions of the interaction potential between argon and the hydroxyl radical in the ground $X\,^2\Pi_{3/2}$ and excited $A\,^2\Sigma^+$ electronic states. Vibrational excitation of the OH moiety may induce dissociation of the complex, providing a means to probe the dynamics taking place on these potential-energy surfaces.[12] The results have shown surprising differences, in both the potentials and the dynamics, between the ground and excited electronic states.

In earlier experiments performed in supersonic jets,[10–15] vdW vibrational progressions associated with the OH–Ar complex were identified in the OH $A\,^2\Sigma^+$–$X\,^2\Pi_{3/2}$ 0–0 and 1–0 regions as well as in the 1–1 and 1–2 regions, the latter cases originating from OH–Ar complexes containing OH

[a)] Alfred P. Sloan Research Fellow and Camille and Henry Dreyfus Foundation Teacher-Scholar.

 0021-9606/90/116469-11$03.00

vibrational excitation in the ground electronic state. A spectroscopic analysis of the OH–Ar vdW stretching progression in the 0–0 region indicated an almost order-of-magnitude increase in the gas phase binding energy of Ar to OH and a decrease in the equilibrium OH–Ar bond length from 3.6 to 2.9 Å upon electronic excitation. The intermolecular potentials derived for OH–Ar complexes in the gas phase show remarkable similarities to the matrix results.

The vast changes in the OH–Ar interaction potential with electronic excitation of the OH radical are also manifested in the dynamics occuring on these surfaces.[12] The rate of vibrational predissociation in OH–Ar complexes is found to be at least five orders of magnitude faster in the excited electronic state. This points to an increased coupling between the OH and vdW stretching motions in the excited state. The increased coupling is also detected spectroscopically by a shift of the OH vibrational frequency in OH–Ar (*vide infra*). These results are consistent with earlier collisional studies on vibrational relaxation of the OH radical by argon, where vibrational energy transfer cross sections were found to be more than 200 times larger in the excited A state than in the ground X state.[20]

In a different type of gas phase experiment, Rostas and co-workers[17] have observed an emission spectrum following laser photolysis of D_2O in high-pressure argon which they ascribe to excimer bands of OD–Ar. The emission is attributed to transitions from vibrationally relaxed levels in the excited state correlating with OD $A\,^2\Sigma^+(v'=0)+\mathrm{Ar}(^1S_0)$ to dissociative regions of the ground-state surface. Good overlap with the dissociative continuum would be expected from the large change in the equilibrium vdW bond length. The OD–Ar emission spectrum is very different from the dispersed fluorescence spectra recorded in the jet from excited vdW levels of the OH–Ar complex, as discussed below.

In this paper, we report the fluorescence excitation spectra of OH–Ar complexes in the vicinity of the OH $A\,^2\Sigma^+$–$X\,^2\Pi_{3/2}$ 0–0, 1–0, 1–1, 2–1, 1–2, and 2–2 transitions. Analysis of the vibrational progressions in the OH–Ar vdW stretching mode of the excited electronic state allowed evaluation of the OH–Ar stretching potentials correlating with OH radicals in the $X\,^2\Pi_{3/2}$ ($v''=0$) and $A\,^2\Sigma^+$ ($v'=0$, 1, and 2) states. A remarkable change in the potential is apparent upon electronic excitation of the OH moiety but relatively small differences occur when the OH subunit is vibrationally excited. Dispersed fluorescence spectra and rotational linewidth measurements have been used to examine the vibrational predissociation dynamics of OH–Ar complexes prepared with one quantum of OH vibrational excitation in the A electronic state. The OH product rotational state distributions are found to reflect the bending wave function of the initially excited vdW level in the OH–Ar complex, thereby revealing the anisotropy of the excited state potential energy surface. In addition, a dramatic change in the vibrational predissociation lifetime of the pure van der Waals stretching levels is observed as a function of the number of quanta of vdW stretch (v_{vdW}). The spectroscopic and dynamical results are discussed in the context of the OH–Ar intermolecular potentials. The experimental results are then compared with recent *ab initio* calculations.[21,22]

EXPERIMENTAL

The experimental method used to produce and detect OH–Ar vdW complexes has been described elsewhere.[11] Briefly, OH radicals are produced by photolyzing nitric acid in argon carrier gas (20–120 psi) with the output of an ArF excimer laser. Photolysis occurs as the gas mixture passes through or exits from a quartz capillary (1 cm long, 0.5 mm bore) which is affixed to the end of a General Valve pulsed valve. The nozzle source produces OH radicals and OH–Ar complexes which are rotationally cold but have significant populations in levels with $v''_{\mathrm{OH}}=1$ and 2.[23] The rotational temperature and, to some extent, the vibrational temperature can be controlled by adjusting the position of the photolysis laser within, or downstream of, the quartz capillary.

The complexes are probed in the 280–360 nm region using the frequency doubled output (Kiton Red or C540A) or the fundamental output (DMQ) of a XeCl excimer pumped dye laser. The frequency doubled laser bandwidth (0.15 cm^{-1}) is narrowed to 0.10 cm^{-1} using an intracavity etalon for those scans used in the rotational analysis and vibrational predissociation lifetime measurements. Frequency doubled pulse energies as great as 1.2 mJ (20 ns) may be achieved but high-pulse energies power broaden the rotational lines of the stronger transitions. Lower energies are chosen to reduce power broadening when rotational resolution is desired and for measurements of relative intensities and spectral linewidths. The laser-induced fluorescence is dispersed by a 0.25 m monochromator (PTI) and detected with a blue-sensitive photomultiplier tube (Thorn EMI 9813Q).

RESULTS

Excitation spectra

Fluorescence excitation spectra of OH–Ar complexes have been observed in the vicinity of the OH $A\,^2\Sigma^+$–$X\,^2\Pi_{3/2}$ 0–0, 1–0, 1–1, 2–1, 1–2, and 2–2 transitions. As an example, a scan of the 1–0 region is shown in Fig. 1. In addition to the well-characterized OH $P_1(1)$, $Q_1(1)$, and $R_1(1)$ lines, a series of new spectroscopic features attributed to complexes of OH with Ar are observed. Each of the transitions in this region involve the promotion of the OH moiety from the ground electronic state with no vibrational excitation to the excited electronic state with one quantum of OH vibration, $v'_{\mathrm{OH}}=1$.

The features labeled 1 to 6 in Fig. 1 have been assigned to a vibrational progression in the OH–Ar vdW stretching mode ($v'_{\mathrm{vdW}}=1$–6) of the excited electronic state correlating with OH $A\,^2\Sigma^+(v'=1)+\mathrm{Ar}(^1S_0)$. In addition to the members of the 1–0 progression shown, the weak vdW origin band $(A,v'_{\mathrm{OH}}=1,v'_{\mathrm{vdW}}=0 \leftarrow X,v''_{\mathrm{OH}}=0,v''_{\mathrm{vdW}}=0)$ has been identified at 34 748.0 cm^{-1} (Fig. 2). Features A–D are also attributed to OH–Ar but have different rotational structure and likely involve bending vibrations. All of the OH–Ar bands in Fig. 1 are analogous in relative position and rotational structure to features previously identified in the OH 0–0 region.[10,11]

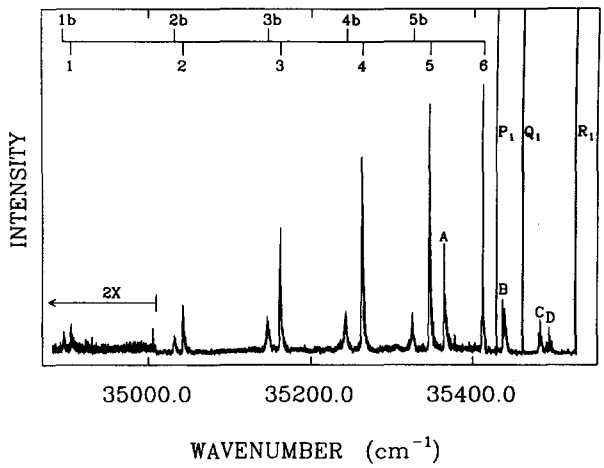

FIG. 1. Fluorescence excitation scan of the OH A–X 1–0 region showing a vibrational progression (labeled 1–6) in the vdW stretching mode of OH–Ar in the A state. Features A–D involve bending vibrations of the OH–Ar complex and 1b–5b are attributed to a vibrational progression in higher order clusters, OH–Ar$_n$ with $n \geqslant 2$. The lines labeled P_1, Q_1, and R_1 are the $P_1(1)$, $Q_1(1)$, and $R_1(1)$ lines in free OH.

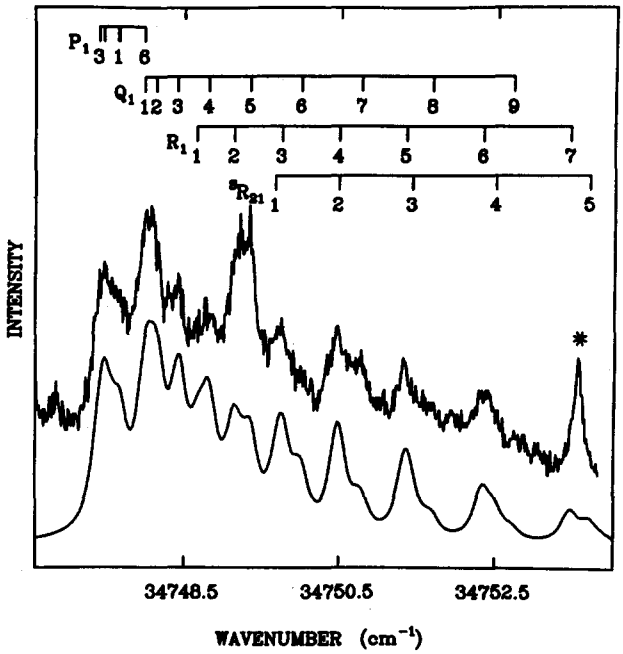

FIG. 2. Fluorescence excitation scan of the origin feature (A,$v'_{OH} = 1$, $v'_{vdW} = 0 \leftarrow X$, $v''_{OH} = 0$, $v''_{vdW} = 0$) in the vdW progression of OH–Ar (upper trace). The lower trace is a simulation using the rotational constants given in Table V. Intensities and bandwidths were simulated using Hönl-London factors for a $^2\Sigma^+ \leftarrow {}^2\Pi_{3/2}$ transition, a temperature of 4 K and a 0.24 cm^{-1} (FWHM) Voight linewidth with a 0.10 cm^{-1} contribution from the laser bandwidth. The asterisk labels the overlapping 1–0 Q_1 (16) transition in free OH.

In each spectral region, there are broad satellite features shifted to lower energy of the elements of the main OH–Ar progression (1b–5b in Fig. 1). These satellites, unlike the main progression bands, show no resolvable rotational structure at the 0.10 cm^{-1} laser bandwidth. They are not hot bands arising from an excited vdW level in the ground electronic state since the spacing from the main progression features is not constant. Additionally, the intensities of these bands relative to the main progression features are maximized under more severe cooling conditions (higher Ar backing pressures and photolyzing higher in the capillary), suggesting that they arise from higher-order clusters, OH–Ar$_n$ ($n \geqslant 2$).

The positions of the main progression features, associated satellites, and features A–D are given in Tables I, II, and III. Calibration is to nearby OH rotational lines, whose absolute frequencies are taken from Crosswhite[24] and Coxon.[25] The vibrational quantum number assignment has been made by analogy to similar vibrational progressions observed upon electronic excitation of hydroxyl radicals imbedded in a solid Ar matrix.[18,26] The absolute frequencies of the transitions for the gas phase OH–Ar complex are substantially shifted from those observed for matrix isolated OH,[27] but the relative spacings and Franck–Condon profile provide an unambiguous correlation between the gas phase and matrix results.

Spectral analysis

A spectroscopic analysis of the rotational and vibrational structure of the main progression features has been performed to evaluate the OH–Ar vdW stretching potentials correlating with OH radicals in the $A\,^2\Sigma^+$ ($v' = 0$, 1, and 2) states. Birge–Sponer plots of the main progression features

TABLE I. Positions[a] (G/cm^{-1}) and relative spacings (ΔG/cm^{-1}) of experimentally observed OH–Ar features in the vdW stretching progressions about the OH A–X transitions.

OH A–X	0–0		1–0		1–1		2–1		1–2		2–2	
v_{vdW}	G	ΔG	G	ΔG	G	ΔG	G	ΔG	G	ΔG	G	ΔG
0	···		34 748.0		···		···		···		···	
1	31 944.3	···	34 905.0	157.0	···	···	···	···	···	···	···	···
2	32 078.4	134.1	35 042.7	137.7	31 474.9	···	34 271.9	···	···	···	···	···
3	32 194.1	115.7	35 162.5	119.8	31 594.7	119.8	34 390.5	118.6	···	···	···	···
4	32 291.8	97.7	35 264.0	101.5	31 696.2	101.5	34 491.4	100.9	28 293.6	···	31 088.4	···
5	32 371.4	79.6	35 347.0	83.0	31 779.2	83.0	34 574.8	83.4	28 376.5	82.9	31 172.1	83.7
6	32 432.8	61.4	35 412.3	65.3	31 844.6	65.4	34 638.2	63.4	···	···	31 235.5	63.4

[a] Measured at the peak of the Q_1 branch to ± 0.1 cm^{-1}.

TABLE II. Positions[a] (G/cm^{-1}) and relative spacings ($\Delta G/cm^{-1}$) of broad features in the region of the OH A–X transitions.

OH A–X	0–0		1–0		1–1		2–1	
v_{vdW}	G	ΔG	G	ΔG	G	ΔG	G	ΔG
1b	···		34 896		···		···	
2b	32 074	···	35 032	136	31 465	···	34 233	···
3b	32 186	112	35 147	115	31 580	115	34 367	134
4b	32 279	93	35 244	97	31 677	97	34 464	97
5b	32 357	78	35 326	82	31 759	82	34 547	83

[a] Measured at the center of each feature to $\pm 1\ cm^{-1}$.

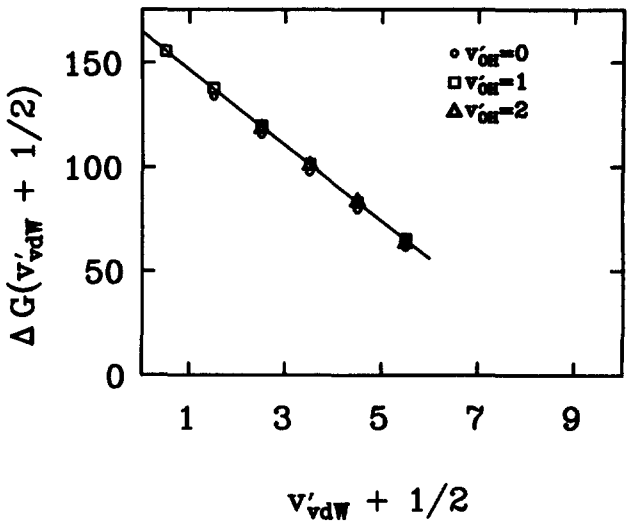

FIG. 3. Birge–Sponer plot of the spacing between the vdW stretching levels (ΔG) in the $v'_{OH} = 0,1$, and 2 wells of the excited A electronic state of OH–Ar vs $(v'_{vdW} + 1/2)$, where v'_{vdW} is the vdW stretching vibrational quantum number.

are shown in Fig. 3. The linearity of the plots indicates that a simple anharmonic oscillator characterizes the vdW stretching motion over most of each potential well. The Birge–Sponer analysis is used to provide the fundamental vibrational frequencies ω'_e and anharmonicities $\omega'_e\chi'_e$ of the OH–Ar vdW stretch (Table IV). Little change in the vdW vibrational parameters occurs upon vibrational excitation of OH within the excited state.

The rotational structure of the vibronic bands in the OH–Ar stretching progressions observed in the OH A–X 0–0, 1–0, and 1–1 regions has been analyzed assuming a linear geometry[11,14] for OH–Ar in the ground and excited states. The rotational structure was well fit by this model but the rotational analysis is not sensitive to the position of the hydrogen atom. A least-squares fit of the calculated P_1, Q_1, R_1, and $^sR_{21}$ rotational line positions to the experimental values yields the rotational constants given in Table V (columns labeled $v_{OH} = 0$ and 1). A total of 267 experimentally measured rotational line positions from the $v'_{vdW} = 1$–6 features in the 0–0 and 1–0 regions were included in a simultaneous fit yielding a standard deviation of 0.023 cm^{-1}, less than one-quarter of the etalon-narrowed laser bandwidth. The rotational line positions from the 1–1 bands (46 lines) are known less accurately and were included in a separate fit, in which the excited state rotational constants were fixed to the values determined in the 0–0 and 1–0 analysis. This yielded a rotational constant for the $X, v''_{OH} = 1, v''_{vdW} = 0$ state. The errors associated with each of the rotational constants represent the scatter in values determined from combination difference analyses. The values for the excited state $v'_{OH} = 2$ levels were evaluated from contour fits of OH–Ar features in the 2–1 region, while the rotational constant for $v''_{OH} = 2$ was previously determined from infrared vibrational overtone spectroscopy.[13]

The quality of the fit is illustrated in Fig. 4, where the calculated line positions are displayed above the experimental spectra for transitions to the $v'_{vdW} = 5$ level in the 0–0, 1–0, and 1–1 regions. The rotational constants for each of these three transitions are very similar (Table V) and the single set of line position labels applies to all three spectra. The 1–1 spectrum is power broadened since high laser powers (> 1 mJ/pulse) were used to detect signals arising from the more sparsely populated $X, v''_{OH} = 1$ state.

Improved signal-to-noise and higher resolution have allowed the evaluation of previously undetermined rotational constants, including those from several newly identified bands, and more precise determination of previously reported values. Our earlier work did not include the rotational constants for the $v_{OH} = 1$ levels in the ground and excited states or for the $v'_{OH} = 0$, $v'_{vdW} = 1$ and 6 levels in the excited state. The rotational constants obtained for the $v'_{OH} = 0$,

TABLE III. Transition energies[a] (G/cm^{-1}) of OH–Ar features A–D and their positions (cm^{-1}) relative to the vdW vibrational origins ($v_{vdW} = 0$).

OH A–X	0–0		1–0		1–1		2–1	
	G	Relative position[b]	G	Relative position	G	Relative position	G	Relative position[b]
A	32 401	609	35 365	616	31 798	617	34 584	606
B	32 465	673	35 438	689	31 871	690	34 660	682
C	32 502	710	35 483	734	31 915	734	34 706	728
D	32 534	742	35 496	747	31 928	747	34 715	737

[a] Measured at the center of each feature to $\pm 1\ cm^{-1}$.
[b] Origin position determined by extrapolation from observed features in the vdW stretching progressions.

TABLE IV. Vibrational parameters (cm^{-1}) for the OH–Ar vdW stretching mode in the ground and excited electronic states.

	Ground state	Excited state		
v_{OH}	0	0	1	2
ω_e	23–33	170	174	174
$\omega_e x_e$	···	9	9	9
D_0	>93	>742[a]	···	···
ΔD_0[b]	···	···	+32	+22

[a] This lower limit is obtained from the last observed bound level (feature D) which lies 742 cm^{-1} above the zero point level. A linear Birge–Sponer extrapolation has given an estimate of $D_0 = 718$ cm^{-1}.

[b] $\Delta D_0 = D_0(v_{OH}) - D_0(v_{OH} = 0)$.

$v'_{vdW} = 2$–5 levels in the current fit differ by less than 0.002 cm^{-1} from those determined in our earlier work[11] but are presented here as better measurements having been obtained from higher resolution spectra and more line assignments. Fawzy and Heaven[14,15] have analyzed several of the bands in the 0–0 and 1–0 progressions, extracting rotational constants for $v''_{OH} = 0$; $v'_{OH} = 0$, $v'_{vdW} = 2$–6; and $v'_{OH} = 1$, $v'_{vdW} = 2$–5. The values they report are consistently lower than those reported here but differ by less than the sum of the stated errors in each measurement.

As expected from the large change in the equilibrium OH–Ar vdW bond length upon electronic excitation, the vdW vibrational origin band in the OH 1–0 region is extremely weak in intensity and was not found in initial spectral scans. The results of the vibrational and rotational analyses of the $v'_{vdW} = 1$ to 6 features in the 1–0 region, however, suggested that if the vibrational quantum numbering scheme were correct, the origin band should appear around 34 749 cm^{-1} and that the excited state vibrationally averaged rotational constant should be 0.166 cm^{-1}. A renewed search of this spectral region revealed an additional band, shown in Fig. 2, at 34 748.0 cm^{-1} with an excited-state rotational constant of 0.166 ± 0.002 cm^{-1}. This band has therefore been assigned to the vdW vibrational origin of the 1–0 progression. To date, the vdW vibrational origin bands associated with other OH A–X transitions have not been observed.

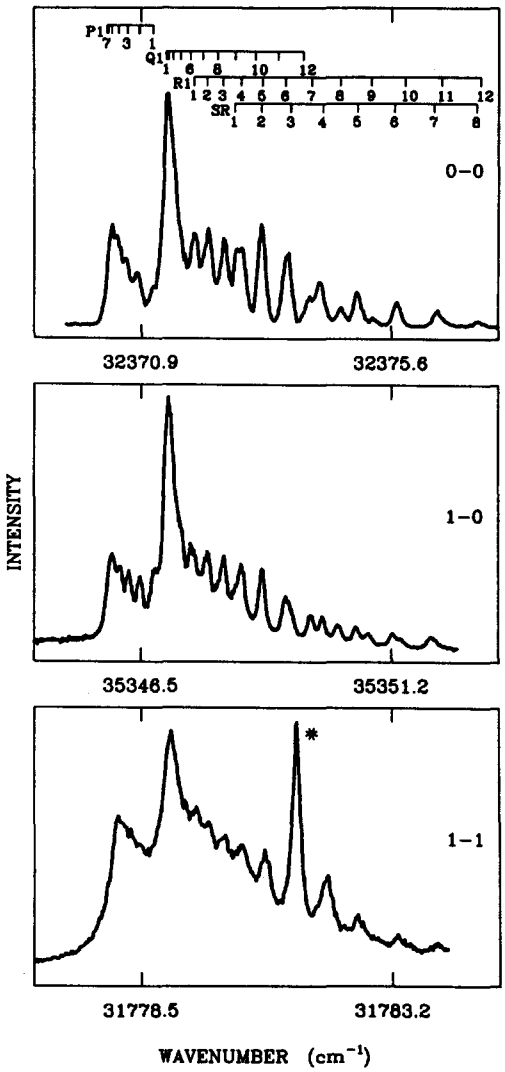

FIG. 4. Fluorescence excitation scans of the OH–Ar $v'_{vdW} = 5$ feature in the 0–0, 1–0, and 1–1 progressions. The asterisk labels the overlapping 0–0 $^0P_{12}(8)$ transition in free OH. Superimposed are the calculated P_1 (≡P1), Q_1 (≡Q1), R_1 (≡R1), and $^sR_{21}$ (≡SR) line positions relevant to all three spectra.

TABLE V. Rotational constants (B_v/cm^{-1}) for OH–Ar in the ground and excited states.

		$v_{OH} = 0$	$v_{OH} = 1$	$v_{OH} = 2$
$X, v_{vdW} =$	0	0.103(1)	0.102(3)	0.101(3)[a]
$A, v_{vdW} =$	0	···	0.166(2)	···
	1	0.164(2)	0.160(2)	···
	2	0.156(2)	0.153(2)	···
	3	0.148(2)	0.144(3)	···
	4	0.138(2)	0.135(3)	(0.135)[b]
	5	0.128(2)	0.127(2)	(0.125)[b]
	6	0.115(2)	0.114(1)	···

[a] Ref. 13.

[b] Obtained from contour fit of low resolution spectrum (± 0.005 cm^{-1}).

The relative integrated intensities of the OH–Ar features in the 1–0 region were measured and are listed in Table VI. Though the spectra were recorded at low laser powers, there is some indication that the Q_1 branch of the $v'_{vdW} = 5$ feature is partially saturated. Since the intensity of the $v'_{vdW} = 4$ feature is nearly as great as that of $v'_{vdW} = 5$, the relative intensities for both $v'_{vdW} = 4$ and 5 are reported only as lower limits. The intensities seen in Fig. 1 do not reflect the tabulated values, since this scan was recorded at higher laser powers which saturate the stronger transitions.

Dispersed fluorescence

Dispersed fluorescence spectra were recorded following excitation of OH–Ar in the 0–0 region. Emission occurs

TABLE VI. Relative integrated intensities, I, of OH–Ar features in the OH A–X 1–0 region.

v'_{vdW}	I
0	1
1	5
2	26
3	83
4	>211
5	>217
6	86

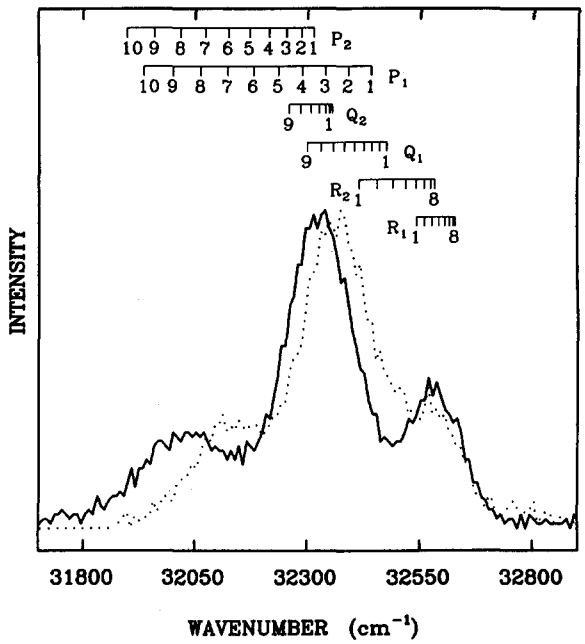

FIG. 5. Dispersed emission from OH $A(v'=0)$ products on the 0–0 transition which result from vibrational predissociation of OH–Ar following excitation of $v'_{vdW}=6$ (dotted line) and feature A (solid line) in the 1–0 region. The labels indicate the main branch OH transitions which contribute to the emission spectrum.

from the complex itself since the vibrational predissociation channel is energetically closed. The spectrum shows two peaks followed by a tail extending to longer wavelengths. These features correspond to bound-bound transitions terminating on the two components of the ground electronic state and bound-free transitions to the ground-state continuum. The separation between the two bound-bound transitions is $120 \pm 15\ cm^{-1}$, where the accuracy is limited by the monochromator resolution. For a linear OH–Ar geometry, this separation would be the spin–orbit splitting in the ground state and is found to be the same as the spin–orbit splitting in uncomplexed OH[24] within the accuracy of this measurement.

The vibrational predissociation dynamics of OH–Ar complexes in the excited electronic state was examined by dispersing the induced fluorescence resulting from preparation of the complex with one or more quanta of OH vibrational excitation, $v'_{OH}>0$. This may lead to vibrational predissociation of the complex, since even one quantum of OH vibration contains more than sufficient energy to break the OH–Ar bond. OH–Ar transitions in the 1–0, 1–1, and 1–2 regions result exclusively in 0–0 emission from the OH $A\,^2\Sigma^+(v'=0)$ products. Similarly, transitions in the 2–1 and 2–2 regions result in 1–0 and 1–1 emission from the OH $A\,^2\Sigma^+(v'=1)$ products. Since no emission is detected from the undissociated complex, OH–Ar must undergo vibrational predissociation on a time scale that is rapid compared to its radiative lifetime.[12]

At $100\ cm^{-1}$ resolution, the dispersed fluorescence spectra of the OH $A\,^2\Sigma^+(v'=0)$ products resulting from excitation of the $v'_{vdW}=3$–6 levels of the A, $v'_{OH}=1$ state are indistinguishable.[12] Although the rotational distribution could not be uniquely determined at this resolution, it was apparent that the population of OH product rotational levels deviates from a Boltzmann distribution and cuts off abruptly after $N=7$. In the present study, excitation of features A and B in the 1–0 region was found to yield emission spectra which are similar to one another but are qualitatively different from those observed after excitation of the pure vdW stretching modes ($v'_{vdW}=3$–6). The fluorescence resulting from excitation of the $v'_{vdW}\leqslant 2$ levels or features C and D is too weak to disperse. Figure 5 shows a comparison of the dispersed emission after excitation of $v'_{vdW}=6$ (dotted line) and of feature A (solid line). The P branches of the OH dispersed emission spectrum extend out further following excitation of feature A, showing that the OH fragments are produced with significant population in higher rotational levels, $N=8$ and 9. A shift in the emission maximum toward lower energy is also observed, which indicates a minimum in the population distribution at low N.

Spectral linewidths

Limits for the vibrational predissociation lifetime of the A, $v'_{OH}=1$, $v'_{vdW}=3$–5 levels of OH–Ar were previously established[12] as $10\ ps \leqslant \tau_{vp} \leqslant 10\ ns$. The lower limit was determined from the laser-limited spectral bandwidth of the 1–0 excitation features. Higher resolution ($0.10\ cm^{-1}$) excitation scans of the seven features in the 1–0 region which correspond to excitation of the complex to the A, $v'_{OH}=1$, $v'_{vdW}=0$–6 levels indicate that some of the bands are indeed, lifetime broadened, allowing narrower limits on the vibrational predissociation lifetimes to be established. Attenuated dye laser powers were used for the $v'_{vdW}=3$–6 levels since they may be easily power broadened. Main branch OH lines provide a good diagnostic of power broadening. OH–Ar may be assumed to have a similar electronic transition strength to OH, with the total transition strength for the complex reduced by the non-unity Franck–Condon factors involving the vdW modes. Main branch OH lines are therefore expected to saturate faster than the OH–Ar transitions and exhibit power broadening at lower laser powers.

As seen in Table VII, the $v'_{vdW}=6$ excitation feature has a spectral linewidth of $0.10 \pm 0.02\ cm^{-1}$ (full width at half-maximum, FWHM) and exhibits no lifetime broadening.

TABLE VII. Spectral linewidths (FWHM), homogeneous contributions to the linewidth (Γ), and vibrational predissociation lifetimes (τ_{vp}) of the OH–Ar main progression features in the OH 1–0 region.

v'_{vdW}	FWHM (cm^{-1})	Γ (cm^{-1})	τ_{vp} (ps)
0	0.24(4)	0.140–0.233	23–38
1	0.28(2)	0.210–0.255	21–25
2	0.27(7)	0.140–0.297	18–38
3	0.30(5)	0.199–0.308	17–27
4	0.20(4)	0.090–0.189	28–59
5	0.12(2)	<0.064	>83
6	0.10(2)	<0.034	>156

Deconvoluting the homogeneous linewidth Γ, from a Voight profile that is at most 0.12 cm^{-1} wide (with a 0.10 cm^{-1} Gaussian contribution from the laser bandwidth) gives an upper limit for $\Gamma \leqslant 0.034$ cm^{-1}. This yields a lower limit for the vibrational predissociation lifetime, $\tau_{vp} \geqslant 156$ ps. The $v'_{vdW} = 5$ level shows a spectral linewidth of 0.12 ± 0.02 cm^{-1} indicating the possibility of homogeneous broadening. However, since the laser bandwidth is included within the error range, we can again establish only a lower limit for the vibrational predissociation lifetime. A Voight linewidth that is at most 0.14 cm^{-1} gives $\Gamma \leqslant 0.064$ cm^{-1} and $\tau_{vp} \geqslant 83$ ps.

The $v'_{vdW} = 0$ through 4 excitation features clearly exhibit homogeneous broadening, corresponding to vibrational predissociation lifetimes for these levels on the order of 10 to 50 ps. Homogeneous broadening is readily seen in Fig. 6,

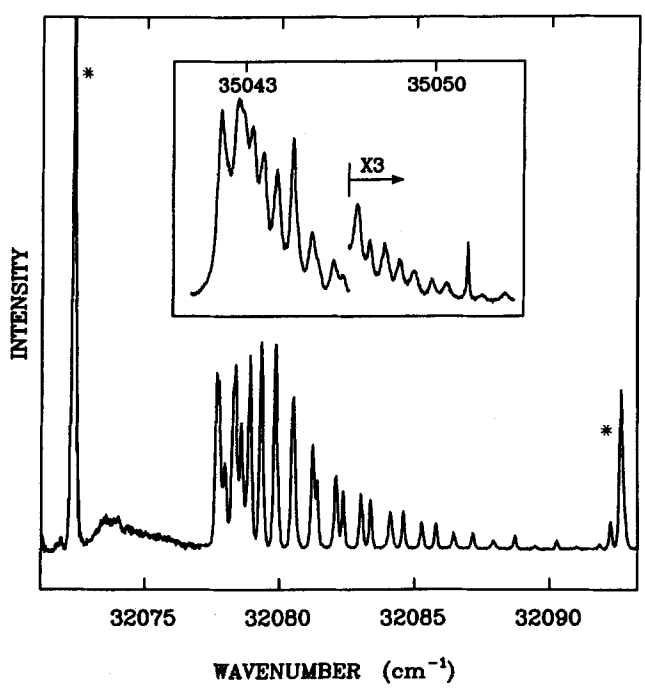

FIG. 6. Fluorescence excitation scans of the OH–Ar $v'_{vdW} = 2$ features in the 0–0 and 1–0 regions. The feature in the 1–0 region (inset) exhibits lifetime broadening as a result of the rapid vibrational predissociation in the excited state. The broad feature centered at 32 074 cm^{-1} is attributed to a higher order cluster (feature 2b in Table II). The asterisks identify nearby transitions of free OH.

by comparing the $v'_{vdW} = 2$ feature in the 0–0 and 1–0 regions. The differences are due to an increase in the linewidth, rather than changes in the rotational constants (Table V). For most of the features ($v'_{vdW} = 0$, 1, 3, and 4) there are no fully resolved, unblended rotational lines from which the linewidth may be measured directly. Therefore, the contour must be simulated using a Voight line profile in order to extract the homogeneous linewidth. This procedure may result in errors as large as $\pm$ 0.05 cm^{-1} in the linewidth. Additionally, for $v'_{vdW} = 2$ there is an indication of a rotational level dependence in the lifetimes. The unblended $^sR_{21}$ lines terminating on $N' = 7$, 8, 9, and 11 show a clear 0.22 ± 0.02 cm^{-1} FWHM, but the P_1 bandhead ($N'' = 2$ and 3) and the low N'', $Q_1(N'')$ and $R_1(N'')$ lines are best simulated with a 0.32 ± 0.02 cm^{-1} linewidth. This provides limits for the vibrational predissociation lifetime of the $v'_{vdW} = 2$ level ($N' \leqslant 11$) of 18 ps $\leqslant \tau_{vp} \leqslant$ 38 ps. These results show a trend of rapidly decreasing lifetime as v_{vdW} decreases from 6 to 3, whereafter (3 to 0) little change in the lifetime is evident.

DISCUSSION

OH $A^2\Sigma^+ + Ar(^1S_0)$ potential

Previously, a Morse potential curve was constructed from the spectroscopic results to represent the OH $A(v' = 0) + Ar(^1S_0)$ intermolecular potential along the OH–Ar vdW stretching coordinate.[11] The potential was defined by the vdW vibrational frequency ω'_e, the binding energy D'_0, and r'_e, the vdW bondlength at the equilibrium position of the well. The vibrational frequency and binding energy were estimated by a Birge–Sponer analysis of the OH–Ar vdW stretching progression in the 0–0 region. The linearity of the Birge–Sponer plot (Fig. 3) indicated that the interaction potential was indeed Morse-like over the spectroscopically accessed region and determined ω'_e and D'_0 to be 170 and 718 cm^{-1}, respectively. The equilibrium bondlength, $r'_e = 2.9$ Å, was derived from the vibrationally averaged rotational constants, B'_v.

The estimate of $D'_0 = 718$ cm^{-1} relied upon a linear extrapolation of the spacing between vdW levels beyond the last observed pure stretching level ($v'_{vdW} = 6$) to the dissociation limit. The last observed bound level (feature D), however, lies 742 cm^{-1} above the zero point level and therefore provides an absolute lower limit for the binding energy. This value is slightly higher than the estimate from the Birge–Sponer extrapolation. The interaction potential in the stretching coordinate is thus very Morse-like through the $v'_{vdW} = 6$ level (641 cm^{-1}), whereafter it shows some positive deviation from the Morse form.

A similar analysis has been performed in this study for the states correlating with the OH $A^2\Sigma^+$ ($v' = 1$ and 2) levels. The Birge–Sponer plots for these wells are also linear (Fig. 3), again indicating the Morse-like behavior of the potentials along the vdW stretching coordinate. This analysis was not used to estimate the binding energy in these states, since deviation from the Morse form is expected near the top of the well. Instead, the spectroscopic shifts of the vdW vibrational origins were used to evaluate the well depths of

OH–Ar in the $v'_{OH} = 1$ and 2 states relative to $v'_{OH} = 0$, as discussed below in the OH vibrational excitation section.

OH $X^2\Pi_{3/2}$ + Ar($^1S_0$) potential

The original spectroscopic analysis[11] provided less information about the ground-state potential which correlates with OH $X(v'' = 0)$ + Ar($^1S_0$). A Morse curve that approximates the true potential along the OH–Ar stretching coordinate was defined by the ground-state binding energy D''_0, the average vdW bondlength at the zero point level r''_0, and an estimate for the vibrational frequency of the OH-Ar stretch ω''_e. The binding energy of Ar to OH in the ground $X^2\Pi_{3/2}(v'' = 0)$ state can be evaluated from the binding energy in the excited state and the spectroscopic shift of the vdW vibrational origin ($v'_{vdW} = 0$) relative to the $P_1(1)$ line of free OH in either the 0–0 or 1–0 regions, by

$$D''_0(X, v''_{OH} = 0) = D'_0(A, v'_{OH} = 0) - [\text{shift in the 0–0 region}]$$

or

$$D''_0(X, v''_{OH} = 0) = D'_0(A, v'_{OH} = 1) - [\text{shift in the 1–0 region}].$$

If a Birge–Sponer extrapolation were used to provide the binding energy in the excited states the resultant ground state binding energy would be 69 cm^{-1}.[11] However, the lower limit on the binding energy in the $A, v'_{OH} = 0$ state, imposed by the position of feature D in the 0–0 region, gives a lower limit on the ground state binding energy of $D''_0 \geq 93\text{cm}^{-1}$.

The average vdW bond length at the zero point level was determined from the rotational analysis. The rotational constant reported in Table V for the $v''_{OH} = 0$ level in the ground state, 0.103 cm^{-1}, differs from our earlier value, 0.110 cm^{-1}.[11] The present calculation takes into account the correct contribution of spin–orbit coupling as determined by the experimentally measured spin–orbit splitting (120 ± 15 cm^{-1}) in the ground state, and therefore supercedes the earlier value. Infrared overtone spectroscopy has provided an independent check of the rotational constant for OH–Ar in the vibrationless level of the ground electronic state.[13] The revised value corresponds to an OH–Ar bond length (r''_0) of 3.7 Å, defined as $(\langle 1/r^2 \rangle)^{-1/2}$, the average distance from the Ar atom to the OH center of mass.

The vdW stretching frequency in the ground state could not be measured directly since vdW vibrational hot bands have not been observed. An estimate for the ground state ω''_e (110 cm^{-1}) was obtained from ω'_e in the excited state and the ground- and excited-state vdW bondlengths.[11] A much more reliable measure of ω''_e is obtained here from the Franck–Condon profile of the main progression features in the 1–0 region which reflects the width of the ground-state wave function. The ground-state vibrational frequency can be evaluated through a Franck–Condon simulation, since the shape of the excited-state potential at the relevant intermolecular separations is well understood. Calculated[28] Franck–Condon factors are found to be strongly dependent on ω''_e but largely independent of the ground state D''_0. Simulation of the observed intensity profile indicates that the ground state ω''_e lies between 23 and 33 cm^{-1}, a value much lower than previously estimated. This lower value for ω''_e assures that there are excited vdW stretching levels supported by the well, although no transitions originating from these levels are observed at the low temperatures attained in the expansion. For ω''_e in this range, a value of $r''_e = 3.6$ Å is necessary to maintain the experimental value of B''_0 (0.103 ± 0.001 cm^{-1}).

The spectroscopic studies have revealed the changes in the OH–Ar potential upon excitation of the OH moiety from the $X^2\Pi_{3/2}$ to the $A^2\Sigma^+$ state. The binding energy increases by nearly an order of magnitude and the OH (center of mass) to Ar separation distance at the equilibrium position decreases from 3.6 to 2.9 Å when OH is promoted from the X to the A state. Additionally, the vibrational frequency of the OH–Ar vdW stretch is much greater in the excited electronic state, pointing to a marked increase in the steepness of the radial potential. The ground-state well is relatively flat, while the excited-state well varies strongly with the OH–Ar separation distance.

OH vibrational excitation

Vibrational excitation of the OH subunit induces changes in the OH–Ar intermolecular potential which can be detected spectroscopically. The changes in the binding energy of OH–Ar upon vibrational excitation of OH within the ground electronic state are obtained through comparison of the transition energies for OH–Ar in the OH A–X 1–0, 1–1, and 1–2 regions.[13] The differences in the positions of excitation features originating from $v''_{OH} = 0$, 1, and 2, and terminating on common vdW levels of $v'_{OH} = 1$ yield the vibrational frequencies of the OH fundamental and first overtone transitions in the ground electronic state of OH–Ar as 3567.8 and 6970.4 cm^{-1}, respectively. These transitions are shifted 0.6 ± 0.1 and 0.9 ± 0.2 cm^{-1} towards lower energy of the corresponding term energies in free OH.[13] The shifts are a measure of the relative binding energies of Ar to OH in the $v''_{OH} = 0$, 1, and 2 levels of the $X^2\Pi_{3/2}$ state and indicate that the binding energy increases only slightly with vibrational excitation of OH. Equivalently, the small shifts indicate a weak perturbation of the OH vibration upon complexation with Ar, which is consistent with the very long vibrational predissociation lifetimes measured for $v''_{OH} = 1$ and 2 in the ground electronic state ($\geq 6\,\mu$s).[12,13]

The effect of OH vibration on the OH $A^2\Sigma^+$ + Ar($^1S_0$) potential is determined by comparing the OH–Ar fluorescence excitation spectra in the OH A–X 0–0, 1–0, 1–1, and 2–1 regions. The frequency of the OH fundamental in OH–Ar is evaluated from the vibrational origin band ($v'_{vdW} = 0$) of the 0–0 (extrapolated) and the 1–0 progressions, yielding $\Delta G_{1/2} = 2957$ cm^{-1}. This is approximately 32 cm^{-1} lower than the fundamental vibrational frequency in uncomplexed OH (1% change), indicating a strongly enhanced coupling between the OH and vdW

stretching modes as compared to the ground electronic state. It is this coupling which leads to the rapid vibrational predissociation observed in the excited electronic state. The spectral shift also shows that the Ar is 32 cm^{-1} more strongly bound to OH $A\,^2\Sigma^+$ in $v' = 1$ than $v' = 0$. Using a similar procedure in the 1–1 and 2–1 regions, we find that OH–Ar in $A,v'_{OH} = 2$ is 22 cm^{-1} more deeply bound than OH–Ar $A,v'_{OH} = 0$, although somewhat less strongly bound (10 cm^{-1}) than OH–Ar $A,v'_{OH} = 1$. OH–Ar in the $A,v'_{OH} = 2$ state may be perturbed by an electronic curve crossing which occurs near the $v' = 2$ level of the OH $A\,^2\Sigma^+$ state.[29]

Vibrational predissociation

The OH product rotational state distribution which results from excitation of features A or B in the 1–0 region is markedly different from that obtained when OH–Ar is prepared in the pure vdW stretching mode. The change in product state distribution is consistent with the assignment of A and B to excitation of the complex to a bend-stretch combination state involving a single quantum of bend. The population of product rotational levels would be expected to change with initial state selection if the product rotational distribution reflects the bending wave function, $\psi_{bend}(\theta)$, of the initially prepared metastable state of the complex.[30,31] In the limit of a rotational sudden approximation, the initial bending motion of the complex is directly mapped onto rotation of the OH product. The product rotational distribution can then be obtained by projecting the bending wave function onto a basis of OH free rotor states.

The rotational sudden approximation may be viewed semi-classically by considering the torque exerted on the OH fragment by the recoiling Ar atom if the vdW bond were suddenly broken. Each angle of departure would produce OH in a particular rotational state with the final product rotational state distribution being determined by the initial angular probability distribution, $|\psi_{bend}(\theta)|^2$. The product rotational distribution resulting from excitation of a pure vdW stretch ($v_{bend} = 0$) in a linear complex would be expected to uniformly decrease from a maximum near $N = 0$, since departure from a linear geometry exerts no torque on the OH fragment. A $v_{bend} = 1$ state, whose wave function has a node at the equilibrium geometry, would be expected to yield a product state distribution with a minimum at $N = 0$. In addition, an excited bending state should produce OH fragments with higher N populated than would $v_{bend} = 0$ since the complex undergoes greater angular excursions yielding larger torques. The observed OH rotational distribution strongly reflects the initially prepared ψ_{bend}, consistent with the sudden limit.

In actuality, the OH product state distribution arises from a combination of effects including the torque exerted when the Ar "pushes off" the repulsive wall (sudden approximation), the angular dependence of the vibrational coupling, and the forces exerted in the exit channel by the long-range parts of the potential surface.[30–32] The sudden approximation would be expected to be reasonable for OH–Ar since the loss of one quantum of OH vibration releases a large amount of energy to products. The greater the amount of energy disposed in translation, the less important will be exit channel forces—for fast moving particles, weak exit channel forces will make only small changes in the trajectories.[33] If exit channel forces were the overriding factor in determining the OH rotational distribution, the product state distribution would be expected to change with the total energy available to products.[30,34–36] We find that transitions to $v'_{vdW} = 3$–6 all yield similar product state distributions while excitation of feature A, which lies between $v'_{vdW} = 5$ and 6 in energy, is clearly different. Changes in E_{avail} are therefore not responsible for the observed differences in the product state distribution.

Some modulation of the product state distribution by exit channel forces and/or vibrational coupling is nevertheless apparent. All of the distributions show significant populations out to a maximum N value (7 for the pure stretches and 9 for features A and B) whereafter there is a sharp cutoff in population.[37] The bending wave function, on the other hand, shows an exponentially decreasing amplitude as a function of θ and therefore would yield a product state distribution with a smoothly decreasing population toward higher N. Thus, the experimental OH rotational distribution shows the effects of the initially prepared ψ_{bend} but is also influenced by exit channel forces and/or the form of the vibrational coupling.

The dramatic change in the vibrational predissociation lifetime with the number of quanta of vdW stretch for the pure vdW stretching levels of the A, $v'_{OH} = 1$ state in OH–Ar is illustrated in Fig. 7 (Table VII). The levels low in the vdW well predissociate significantly faster than the levels closer to

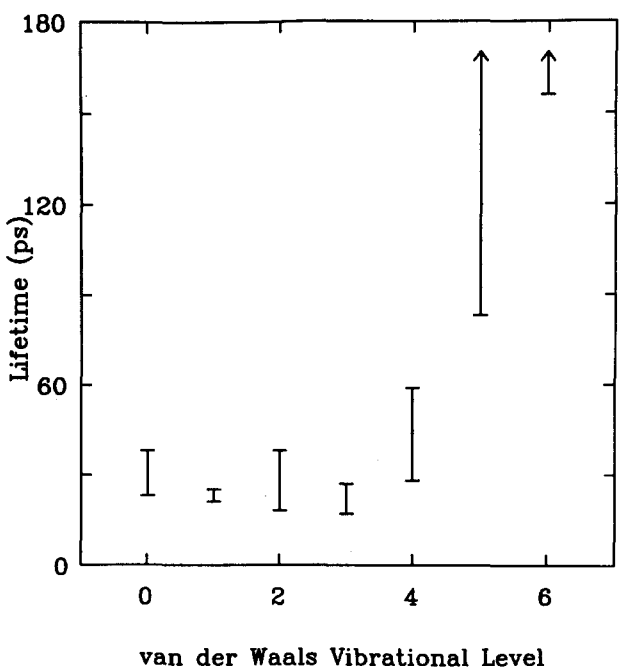

FIG. 7. Vibrational predissociation lifetimes for the pure vdW stretching levels in the $A,v'_{OH} = 1$ state of OH–Ar as a function of vdW vibrational quantum number, v'_{vdW}.

the dissociation limit. This is the trend expected if an "energy gap" or "momentum gap" argument,[38–40] in which the rate depends exponentially on the negative square root of the energy released to translation, were invoked.

The vibrational predissociation lifetimes for different vdW levels were calculated using a Fermi Golden Rule expression,

$$\tau_{vp}^{-1} = (4/\hbar^2 v_m)|\langle \Psi_m^{(0)}|V'|\Psi_n^{(0)}\rangle|^2,$$

where v_m is the relative velocity of the recoiling fragments and V' is the coupling term which connects the initially prepared metastable state ($\Psi_n^{(0)}$ to first order) and the final state of the fragments ($\Psi_m^{(0)}$).[41] An analytical solution to the Golden Rule equation was derived by Beswick and Jortner[38] for two coupled colinear Morse oscillators. Ewing[39] later considered the specific case of triatomic, hydrogen-bonded systems. According to these models the lifetime is given by

$$\tau_{vp}^{-1} = K \exp[-\pi(2\mu\Delta E)^{1/2}/a\hbar],$$

where ΔE is the final translational kinetic energy of the fragments, μ is the reduced mass of the complex, and a ($\propto \omega_e\sqrt{\mu/D_e}$), the Morse range parameter, is a measure of the steepness of the repulsive wall of the vdW potential. The pre-exponential factor K is dependent upon both ΔE and the number of bound vdW levels. In many systems, the exponential term dominates giving the familiar form of the "energy gap" or "momentum gap" law. For the specific case of OH–Ar, however, the large number of bound vdW levels makes this simplification inappropriate. A calculation including the pre-exponential factor failed to reproduce the trend of decreasing vibrational predissociation lifetime with decreasing vdW level in the A state.

A similar calculation was performed comparing the vibrational predissociation lifetimes in the ground and excited electronic states. The difference in ΔE alone is insufficient to reproduce the observed change ($> 10^5$ times faster in the excited electronic state when comparing the $v_{vdW} = 0$ levels in each state). Rather, the enormous change in lifetime must be attributed to differences in the form of the OH–Ar potential.[42] Using the potential parameters derived in this spectroscopic analysis, the calculation yields an up to 40 order-of-magnitude decrease in lifetime upon electronic excitation. The range parameter evaluated from the earlier estimate of ω_e'' and D_0''[11] predicted the opposite trend, with the excited state undergoing predissociation on a somewhat slower time scale than the ground state. This illustrates the extreme sensitivity of the calculated lifetime to potential parameters. The simple model calculation performed here indicates that the difference in observed lifetime is related to the difference in the steepness of the radial potentials. However, the approximations inherent in this model mean that these calculations cannot be interpreted quantitatively. This limitation and the failure of the model calculations to reproduce the lifetime dependence on vdW level in the excited state point to the need for full three-dimensional quantum dynamical calculations to interpret the experimental results.

Ab initio calculations

Recently, Degli Esposti and Werner[21] have calculated three dimensional *ab initio* interaction potentials for Ar ($^1S_0$) with OH $A\,^2\Sigma^+$ ($v' = 0$) and OH $X\,^2\Pi$ ($v'' = 0$). In the excited electronic state correlating to OH $A(v' = 0)$ + Ar, the potential exhibits deep minima in the linear hydrogen-bonded OH–Ar and anti-hydrogen-bonded Ar–OH configurations. The potential is strongly anisotropic, with a high barrier separating the two isomers. The OH–Ar isomer has a well depth of 1100 cm^{-1} at an equilibrium distance of 2.9 Å (identical to the experimental value for r_e'), while the Ar–OH isomer has a comparable well depth (1000 cm^{-1}) at a significantly shorter equilibrium distance of 2.2 Å. The bound-state levels supported by this potential have been calculated by Chakravarty *et al.*,[22] who find a high-frequency excited state bending vibration which makes a sizable contribution ($\sim$440 cm^{-1}) to the zero point energy. The relative positions of the vdW stretching levels for the OH–Ar conformer are in good agreement with the experimental results presented above.

Two different OH–Ar potentials correlate with OH $X\,^2\Pi$ + Ar($^1S_0$), depending on the orientation of the orbital containing the unpaired electron of the OH radical with respect to the OH–Ar plane. The ground electronic state has the orbital containing the unpaired electron in the OH–Ar plane (A'). The *ab initio* calculations predict the minimum ($\sim$100 cm^{-1}) to occur at the linear OH–Ar configuration with a separation distance of 3.8 Å (recall the experimental value, $r_e'' = 3.6$ Å). In contrast to the intermolecular potential in the A state, the ground-state potential is shallow and slowly varying with respect to angle. At the zero point level, the complex is expected to undergo a wide amplitude bending motion. The *ab initio* results confirm the experimental observations of a strongly bound excited-state potential with a minimum that is substantially displaced from the ground state minimum.

Chakravarty *et al.*[22] have also simulated the positions and intensities of features in the ultraviolet excitation spectrum, based solely on the *ab initio* potential surfaces. The theoretical calculation predicts a vdW stretching progression which closely resembles the observed progression in the OH A–X 0–0 region. The spacings between elements are better reproduced, however, if the first observed band in the experimental progression is assigned to $v_{vdW}' = 0$ rather than $v_{vdW}' = 1$, suggesting that the *ab initio* potential in the excited A state is too shallow. Additional bands are predicted to appear in the high-energy region of the spectrum, analogous to the nonprogression features identified in the experimental spectra. The latter are attributed to Fermi resonances, which mix bend or bend-stretch combinations with pure stretching vibrations.

CONCLUSION

The spectroscopic studies of OH–Ar complexes have revealed much information about the interaction potentials of Ar with OH in the ground $X\,^2\Pi_{3/2}$ and excited $A\,^2\Sigma^+$

electronic states. Excitation of the OH stretching mode produces relatively small perturbations in the potentials, while electronic excitation of the OH subunit substantially changes the form of the interaction. The radial part of the intermolecular potential correlating with OH $X^2\Pi_{3/2} + \mathrm{Ar}(^1S_0)$ is determined to be relatively flat, with $D_0'' \geqslant 93\ \mathrm{cm}^{-1}$. In contrast, the well in the excited state is found to be significantly deeper ($D_0' \geqslant 742\ \mathrm{cm}^{-1}$) and to vary strongly with the OH separation distance.

While a standard spectroscopic analysis yielded information about the radial part of the potential, the vibrational predissociation dynamics have given insight into the angular dependence. Product rotational state distributions resulting from excitation of different vdW modes (A, $v'_{\mathrm{OH}} = 1$, v'_{bend}, v'_{vdW}) in the OH–Ar complex have been discussed in the limit of the rotational sudden approximation. Although the observed distributions strongly reflect the bending wavefunction of the initially prepared metastable state, some effect of exit channel forces and/or vibrational coupling is apparent.

Vibrational predissociation lifetimes of the complex have been measured as a function of electronic state and of excited state vdW vibrational level. One would expect that a comparison of the experimental results to exact dynamical calculations will provide a very sensitive test of the accuracy of the *ab initio* potential energy surfaces. Continued interaction between experimentalists and theoreticians promises to lead to an even greater understanding of this benchmark system.

ACKNOWLEDGMENTS

This research was supported by the Division of Chemical Sciences, Office of Basic Energy Sciences of the Department of Energy. M. I. L. gratefully acknowledges the Natural Science Association at the University of Pennsylvania for a Young Faculty Award. We thank H.-J. Werner, D. C. Clary, and G. E. Ewing for stimulating discussions, and W. M. Fawzy and F. Rostas for sharing their results with us prior to publication.

[1]P. D. A. Mills, C. M. Western, and B. J. Howard, J. Phys. Chem. **90**, 3331 (1986).
[2]P. D. A. Mills, C. M. Western, and B. J. Howard, J. Phys. Chem. **90**, 4961 (1986).
[3]P. Andresen, D. Haüsler, and H. W. Lülf, J. Chem. Phys. **81**, 571 (1984).
[4]K. Liu and R. G. Macdonald, J. Chem. Phys. **89**, 4443 (1988).
[5]P. J. Dagdigian, J. Chem. Phys. **90**, 2617 (1989).
[6]V. Aquilanti, R. Candori, and F. Pirani, J. Chem. Phys. **89**, 6157 (1988).
[7]V. Aquilanti, E. Luzzati, F. Pirani, and G. G. Volpi, J. Chem. Phys. **89**, 6165 (1988).
[8]C. H. Becker, P. Casavecchia, and Y. T. Lee, J. Chem. Phys. **70**, 2986 (1979).
[9]M. I. Lester, in *Dynamics of Polyatomic van der Waals Complexes*, edited by N. Halberstadt and K. C. Janda (Plenum, New York, 1989).
[10]M. T. Berry, M. R. Brustein, J. R. Adamo, and M. I. Lester, J. Phys. Chem. **92**, 5551 (1988).
[11]M. T. Berry, M. R. Brustein, and M. I. Lester, Chem. Phys. Lett. **153**, 17 (1988).
[12]M. T. Berry, M. R. Brustein, and M. I. Lester, J. Chem. Phys. **90**, 5878 (1989).
[13]K. M. Beck, M. T. Berry, M. R. Brustein, and M. I. Lester, Chem. Phys. Lett. **162**, 203 (1989).
[14]W. M. Fawzy and M. C. Heaven, J. Chem. Phys. **89**, 7030 (1988).
[15]W. M. Fawzy and M. C. Heaven, J. Chem. Phys. **92**, 909 (1990).
[16]R. K. Lengel and D. R. Crosley, J. Chem. Phys. **68**, 5309 (1978).
[17]J. L. Lemaire, W-U. L. Tchang-Brillet, N. Shafizadeh, J. Rostas, and F. Rostas, J. Chem. Phys. **91**, 6657 (1989).
[18]J. Goodman and L. E. Brus, J. Chem. Phys. **67**, 4858 (1977).
[19]D. R. Crosley, J. Phys. Chem. **93** (1989), and references cited therein.
[20]K. J. Rensberger, J. B. Jeffries, and D. R. Crosley, J. Chem. Phys. **90**, 2174 (1989).
[21]A. Degli Esposti and H-J. Werner (to be published).
[22]C. Chakravarty, D. C. Clary, A. Degli Esposti, and H-J. Werner (to be published).
[23]The present results differ from the earlier work in which little vibrational excitation of the OH product upon photolysis of HNO_3 at 193 nm was reported. A Jacobs, K. Kleinermanns, H. Kuge, and J. Wolfrum, J. Chem. Phys. **79**, 3162 (1983).
[24]G. H. Dieke and H. M. Crosswhite, J. Quant. Spectrosc. Radiat. Transfer **2**, 97 (1962).
[25]J. A. Coxon, Can. J. Phys. **58**, 933 (1980).
[26]Rapid vibrational relaxation of OH–Ar to the lowest level in $v'_{\mathrm{OH}} = 0$ prior to fluorescence assures that the origin feature was correctly identified in the matrix work.
[27]The origin of the 0–0 progression in the matrix is shifted $\sim 246\ \mathrm{cm}^{-1}$ to lower energy of the gas phase value.
[28]R. J. LeRoy supplied the FORTRAN programs used to calculate the eigenvalues and eigenfunctions of a one-dimensional potential and the Franck–Condon factors between levels of two different potentials.
[29]K. R. German, J. Chem. Phys. **63**, 5252 (1975).
[30]R. L. Waterland, M. I. Lester, and N. Halberstadt, J. Chem. Phys. **92**, 4261 (1990).
[31]N. Halberstadt, J. A. Beswick, and K. C. Janda, J. Chem. Phys. **87**, 3966 (1987).
[32]R. Schinke, Annu. Rev. Phys. Chem. **39**, 39 (1988).
[33]In the collisional studies (see Ref. 16) with only $200\ \mathrm{cm}^{-1}$ of excess energy, long-range forces in the entrance channel dominate the dynamics.
[34]J. C. Drobits and M. I. Lester, J. Chem. Phys. **88**, 120 (1988).
[35]J. C. Drobits and M. I. Lester, J. Chem. Phys. **89**, 4716 (1988).
[36]R. L. Waterland, J. M. Skene, and M. I. Lester, J. Chem. Phys. **89**, 7277 (1988).
[37]The observed cutoff is not due to a constraint on available energy.
[38]J. A. Beswick and J. Jortner, Adv. Chem. Phys. **47**, 363 (1981).
[39]G. E. Ewing, J. Chem. Phys. **72**, 2096 (1980).
[40]G. E. Ewing, Faraday Discuss. Chem. Soc. **73**, 325 (1982).
[41]M. S. Child, *Molecular Collision Theory* (Academic, New York, 1974).
[42]G. E. Ewing, private communication.